Journal of Power Sources 195 (2010) 6301–6311

Contents lists available at ScienceDirect

Journal of Power Sources

journal homepage: www.elsevier.com/locate/jpowsour

Structural modifications to nickel cermet anodes in fuel cell environments

Douglas G. Ivey[a,*], Edward Brightman[b], Nigel Brandon[b]

[a] Department of Chemical and Materials Engineering, University of Alberta, Edmonton, Alberta, Canada T6G 2V4
[b] Department of Earth Science and Engineering, Imperial College, London SW7 2AZ, UK

ARTICLE INFO

Article history:
Received 6 March 2010
Received in revised form 16 April 2010
Accepted 19 April 2010
Available online 24 April 2010

Keywords:
Solid oxide fuel cells
Nickel
Ni/YSZ
Ni/CGO
Microstructure
Electron microscopy

ABSTRACT

Restructuring of Ni in cermet anodes of solid oxide fuel cells (SOFCs) has been studied using both bulk fuel cells and thin foil anodes. The bulk cells were button cells (23 mm in diameter) with cermet anodes (30–70 μm thick) made up of nickel and gadolinium-doped ceria (Ni/CGO). The cells were operated (under current load) at 700 °C in moist H_2 or moist H_2 with low levels of H_2S. Scanning electron microscopy (SEM) was used to characterize the microstructure before and after testing. The thin foil samples (100–150 nm thick) were cermets of nickel and yttria doped zirconia (Ni/YSZ) and these were exposed (without current load) at 700 °C to dry H_2, moist H_2 or moist H_2 with H_2S (1 ppm). Transmission electron microscopy (TEM) and SEM were used to analyze the microstructural changes in these samples. The anodes from the bulk cells exhibited terracing of Ni grains in all instances, with the extent of terracing increasing with exposure to H_2S, and with increasing H_2S levels and exposure time. The thin foil anodes showed much more extensive Ni restructuring leading to agglomeration and faceting of Ni grains. This was accompanied by debonding from YSZ, commencing at triple points, where some combination of three Ni/YSZ grains meet. The amount of restructuring increased with increasing H_2 concentration in the gas, and was accelerated by the presence of H_2S and/or H_2O. Evidence is presented that indicates that terracing may represent the early stages of Ni agglomeration.

1. Introduction

Solid oxide fuel cells (SOFCs) are electrochemical devices, which convert the free energy of a chemical reaction directly to electrical energy [1,2]. The fuel supplied to the SOFC need not be pure hydrogen, but can be a hydrocarbon, such as natural gas, coke oven gas and biogas. The use of hydrocarbons requires breaking of the carbon–hydrogen bonds, usually using steam over a nickel catalyst, to produce hydrogen plus carbon monoxide. Carbon monoxide can act as a supplemental fuel, reacting with oxygen ions at the cathode to produce carbon dioxide. The downside to hydrocarbon fuels is that they generally contain impurities, such as H_2S, which can have deleterious effects (even at the ppm level) on cell performance [3].

The anode component of the fuel cell needs to be electronically conducting and electrochemically active. A Ni cermet is typically utilized for this purpose and is essentially a composite material of Ni and yttria-stabilized zirconia (YSZ) or gadolinium-doped ceria (CGO). The Ni, when present in sufficient quantities (40–60 vol.%), provides percolated electron conduction pathways. The ceramic phase (YSZ or CGO) is electronically insulating, but ionically conducting, so that the combination of Ni and the ceramic generates sufficient triple phase boundaries (TPBs), where the fuel gas, ions and electrons are in contact, for efficient fuel cell operation. In addition, the ceramic reduces thermal mismatch between the anode and the electrolyte, and helps provide high temperature structural stability [4].

Anode structural stability is a concern, because Ni has a relatively low melting temperature (1455 °C), making it susceptible to agglomeration and shape change during cell fabrication and subsequent operation [5–8]. Prolonged exposure to fuel gases at elevated temperatures can lead to Ni coarsening or agglomeration resulting in the loss of percolation under some conditions, with a marked drop in anode electrical conductivity, and a reduction in the number of TPBs, reducing electrochemical performance. Zha et al. [6] showed that Ni/CGO/anodes with coarser Ni microstructures exhibited a decrease in peak power densities and an increase in polarization resistance relative to those with finer microstructure. Simwonis et al. [8] have tried to quantify the impact of Ni, using long-term (4000 h) aging of Ni/YSZ anodes in a fuel environment. The electronic conductivity decreased by more than 30%, which was attributed to an increase in the Ni particle size from 2.0 to 2.6 μm. Similar results were reported by Iwata [9] for Ni/YSZ anodes. After cell operation for 1000 h, Ni particles as large as

* Corresponding author at: Department of Chemical and Materials Engineering, University of Alberta, 7th Floor, ECERF Building, Edmonton, Alberta, Canada T6G 2V4. Tel.: +1 780 492 2957; fax: +1 780 492 2881.
E-mail address: doug.ivey@ualberta.ca (D.G. Ivey).

0378-7753/$ – see front matter © 2010 Elsevier B.V. All rights reserved.
doi:10.1016/j.jpowsour.2010.04.059

10 μm were observed compared with as fabricated Ni particles in the 0.1–1.0 μm range. Nickel agglomeration is also enhanced by the presence of water vapour in the fuel gas, although the effect appears to be independent of water concentration [5,8].

As mentioned above, sulphur is a common impurity (e.g., H_2S) in many hydrocarbon-based fuels. At SOFC operating temperatures even very small amounts of sulphur (<1 ppm) can interact strongly with the nickel component of the anode. Sulphur degrades cell performance, likely by deactivating the surface of the nickel particles by surface coverage and accompanying blocking of the active catalytic sites. Bartholomew has reported that greater than 90% coverage of the surface of the nickel particles occurs at H_2S concentrations between 0.1 and 1 ppm at 450 °C [10]. Performance degradation increases as H_2S concentration in the fuel gas is increased, and tolerance to sulphur impurities decreases as the operating temperature is decreased [11–15]. Lohsoontorn et al. [15] also showed that the amount of H_2 in the fuel had an effect; decreasing the H_2 content, from 97 to 9.7%, while keeping the H_2S concentration fixed at 1 ppm, resulted in more pronounced poisoning of Ni/CGO anodes. In the studies cited, recovery, full or partial, was obtained after exposure to fuel containing no sulphur impurities.

Recent work has shown that sulphur can also alter the Ni microstructure. Sasaki et al. [3] have observed anode detachment (for YSZ/Ni systems) from the electrolyte after exposure to 5 ppm H_2S at 800 °C and 200 mA cm^{-2} followed by rapid cooling in pure N_2. Nickel was oxidized to NiO, which the authors attributed to the operating conditions with H_2S.

Lohsoontorn [16] has reported on structural modifications to Ni, in CGO/Ni anodes, exposed at 600 °C for up to 120 h to moist H_2 (97% H_2 and 3% H_2O) with 1–3 ppm H_2S and dry (97% H_2 and 3% N_2) with up to 10 ppm of H_2S. Two effects were observed. Nickel agglomeration was accelerated by the presence of H_2S, and the effect was more pronounced at higher concentrations. Step-like formations (terraces or facets) were also observed on Ni surfaces exposed to H_2S, with the frequency of terracing increasing with increasing H_2S concentration and exposure time. Terracing was not as pronounced for H_2S-containing dry H_2 atmospheres. This effect was not dependent on the ceramic component in the anode, as similar terracing was observed for pure Ni pellets (same temperature) and YSZ/Ni anodes (at 800 °C) [16]. Electrochemical measurements of fuel cells with CGO/Ni anodes at 600 °C showed that degraded cells (due to exposure to H_2S) could be fully recovered using humidified H_2 when the H_2S concentration was 1 ppm; however, full recovery was not possible for 3 ppm H_2S exposure. The unrecoverable part of the performance was attributed by Lohsoontorn [16] to irreversible Ni agglomeration. The effect of Ni terracing on cell performance was less clear; however, electrochemical impedance spectroscopy (EIS) measurements indicated that terracing may slow down the performance degradation rate.

Because of the importance of Ni microstructure in the anode to fuel cell performance, it was decided to investigate the restructuring phenomenon more closely. Bulk anode structures, as well as thin foil anode structures, have been studied in different environments, including dry hydrogen, wet hydrogen and hydrogen with low levels of H_2S. The bulk anodes were Ni/CGO while the thin film samples were Ni/YSZ. A different cermet was used for the thin foil studies because, in part, of its availability. Also, previous work has shown that cermet type does not appear to affect Ni restructuring. Limited tests were done on Ni/CGO thin film samples to confirm similar behaviour. The purpose of the thin foil samples was to accelerate the restructuring kinetics to approximate long-term exposure in the anode. Both scanning and transmission electron microscopy (SEM and TEM) were utilized to characterize the microstructural changes. The focus of this work is microstructure; electrochemical results will be the emphasis of future work.

2. Materials and methods

Two types of samples were characterized in this work: electrolyte supported button fuel cells and separate anode substrates. The three-electrode button cells were fabricated with nickel–gadolinium-doped ceria (Ni-CGO) anodes, yttria-stabilized zirconia (YSZ) electrolytes and lanthanum–strontium–manganite (LSM–YSZ) cathodes and reference electrodes. 8 mol.% YSZ (Tosoh TZ-8Y, Japan) electrolyte powder was uniaxially die-pressed and sintered at 1450 °C for 5 h to give dense pellets 1.25 ± 0.5 mm thick and 23 mm in diameter. Cermet anodes (30–70 μm thick) consisting of 60 wt.% NiO:40 wt.% $Ce_{0.9}Gd_{0.1}O_{1.95}$ (Fuel Cell Materials, USA) were screen printed and sintered at 1350 °C for 1 h. Cathodes and reference electrodes consisting of 50 wt.% $(La_{0.8}Sr_{0.2})MnO_{3-x}$:50 wt.% $(Y_2O_3)_{0.08}(ZrO_2)_{0.92}$ (Fuel Cell Materials, USA) were then screen printed and sintered at 1150 °C for 1 h.

The test rig design was similar to that described in Offer et al. [17]. The anodes of the cells were reduced at 800 °C in a mixture of N_2 and H_2 with 2% steam. After reduction the furnace temperature was reduced to 700 °C for testing. A total flow rate of 100 mL min^{-1} was used and the default gas composition for clean fuel was 49% H_2, 49% N_2 and 2% H_2O. The counter and reference electrodes were supplied with air at a rate of 30 mL min^{-1}. The cells were operated at a current density of 200 mA cm^{-2} for a total of 24–25 h. For samples exposed to H_2S, after ~5 h of operation with clean fuel, the gas composition was changed to contain 0.5 or 1.0 ppm H_2S for 15–18 h. The cells were cooled at open circuit to room temperature in dry H_2/N_2 (10%/90%) or dry N_2. Control samples were run on the clean fuel composition for the entire 24–25 h.

The second type of samples were thin TEM sections prepared from porous Ni/YSZ anode substrates (Ningbo Institute of Material Technology and Engineering, China). The material was supplied in sheet form, approximately 1 mm thick. The NiO/YSZ composite sheet was reduced by heating to 750 °C at a rate of 5 °C min^{-1} in 97% N_2/3% H_2, followed by increasing the H_2 concentration to 97% over a period of 1 h at 750 °C, holding in 97% H_2/3% H_2O for 1 h and finally cooling to room temperature at a rate of 5 °C min^{-1} in 97% N_2/3% H_2. Once reduced, several 3 mm diameter discs were machined from the sheet using a Gatan Model 601 ultrasonic disc cutter. These were then ground and polished on both sides, using progressively finer SiC papers (final step with 1200 grit paper), to a thickness of 80–120 μm and then dimpled (Gatan 656 dimple grinder) on both sides to a central thickness of <15 μm. The dimpled regions received a final polish using 1 μm diamond paste. The samples were sputtered from both sides to electron transparency using a Gatan 691 PIPS precision ion mill. Argon ions (Ar^+) were accelerated towards the sample surfaces using a voltage of 4 kV at an incident angle of 8–10° to the sample surface until a central hole was produced. This was followed by 2.5 kV and 6° for 30–45 min. The latter conditions were utilized to increase the amount of thin area and to reduce ion damage. It should be noted that electron transparent regions were located near the central hole.

TEM samples for ex situ exposure were placed in an alumina boat which was placed in a quartz tube in a horizontal furnace. The samples were heated at 7.5 °C min^{-1} to the exposure temperature (700 °C) in 10% H_2/90% N_2, with a total flow rate of 100 mL min^{-1}. When the desired temperature was reached the gas composition was changed to the desired mixture for exposure. The specific gas mixtures and exposure times are given in Table 1. After the specified exposure time, the gas was changed to pure N_2 and the sample was cooled to <100 °C in 15–20 min.

Fuel cell samples were examined, in both plan view and cross-section orientations, in a Leo Gemini 1525 field emission gun SEM. The SEM was operated at 5 kV with a working distance of 5–6 mm, using the in-lens secondary electron (SE) detector for imaging. For plan view orientations, the bottom surface of the anode was

Table 1
Gas exposure conditions for YSZ/Ni anode thin foils*.

Sample	Atmosphere (vol.%)	Duration (min)
YSZ/Ni	1 ppm H_2S in 100% H_2	5
YSZ/Ni	1 ppm H_2S in 100% H_2	15
YSZ/Ni	1 ppm H_2S in 100% H_2	90
YSZ/Ni	2% H_2/98% N_2	15
YSZ/Ni	10% H_2/90% N_2	15
YSZ/Ni	100% H_2/0% N_2	15
YSZ/Ni	100% H_2/0% N_2	90
YSZ/Ni	2% H_2O/49% H_2/49% N_2	15
YSZ/Ni	1 ppm H_2S in 2% H_2O/98% H_2	15
YSZ/Ni	1 ppm H_2S in 2% H_2O/49% H_2/49% N_2	15
CGO/Ni	1 ppm H_2S in 100% H_2	15

* All exposures were done at 700 °C.

examined, i.e., the surface in contact with the current collector. Cross-section samples were prepared by fracturing in air.

TEM samples were examined in a JEOL 2000FX TEM, operated at 200 kV, and equipped with an Inca energy dispersive X-ray (EDX) system. Selected samples were also examined in an FEI Titan 80/300 TEM/STEM, operated at 300 kV, in order to obtain electron tomographic images. Atomic number (Z) contrast was utilized for this purpose using a high angle, annular dark field (HAADF) detector. A series of images was obtained over the angular range from −60° to +60° in 1° or 2° intervals. Three-dimensional reconstruction was performed using Amira Version 5.2.2 software.

3. Results and discussion

3.1. SEM analysis of CGO/Ni anodes from tested fuel cells

The as reduced anode was examined initially in order to establish a baseline condition. Plan view and cross-section images are shown in Fig. 1. The CGO grains are essentially featureless, while many of the Ni grains have small particles on their surfaces. The particles will be addressed in the next paragraph. Besides the particles, there is no evidence of any Ni surface features, such as terracing.

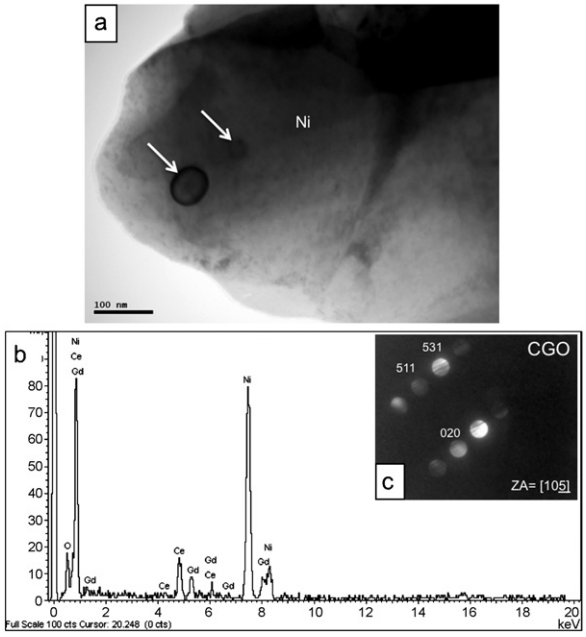

Fig. 2. (a) TEM BF image with arrows indicating particles on a Ni grain, (b) EDX spectrum and (c) microdiffraction pattern from larger particle.

The particles on the Ni surfaces were too small to identify through EDX analysis in the SEM, so a TEM sample was prepared of the anode. Fig. 2 shows a bright field (BF) image of a Ni grain with two particles on the surface (indicated by arrows), as well as an EDX spectrum and a microdiffraction pattern from the larger particle. The EDX spectrum clearly shows the presence of Ce, Gd and O, as well as a strong Ni signal from the surrounding Ni grain. The diffraction pattern can be indexed to CGO, with an orientation close to the $[1\,0\,\bar{5}]$ zone axis. Several diffraction patterns were obtained from other orientations and confirmed that the particles were indeed CGO. The particles then are likely an artifact of the cell fabrication process.

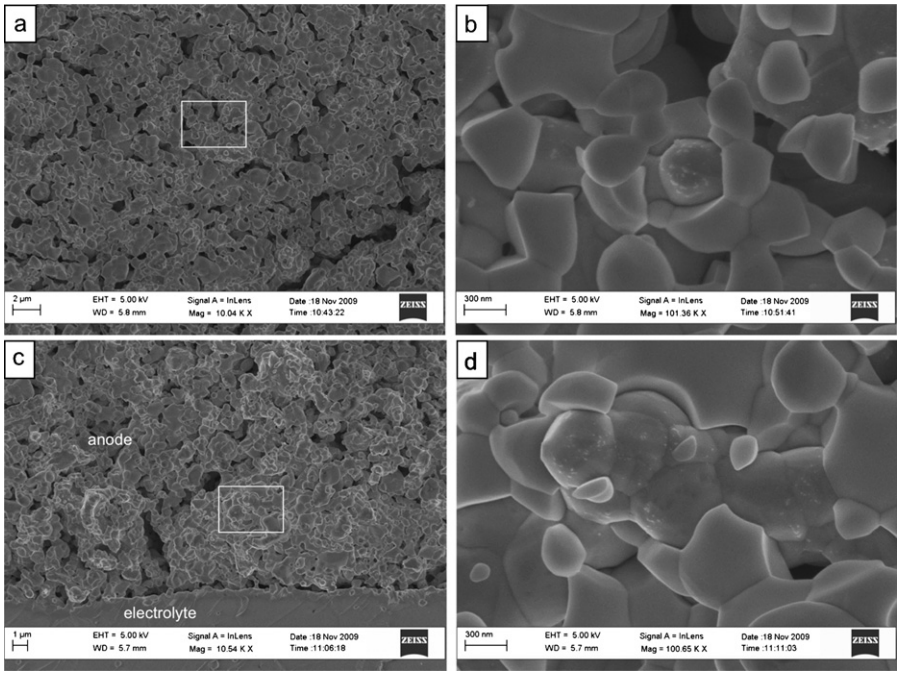

Fig. 1. SEM SE images from an as reduced Ni/CGO anode. (a and b) Plan view images; (b) is a magnified view of the highlighted region in (a). (c and d) Cross-section images; (d) is a magnified view of the highlighted region in (c).

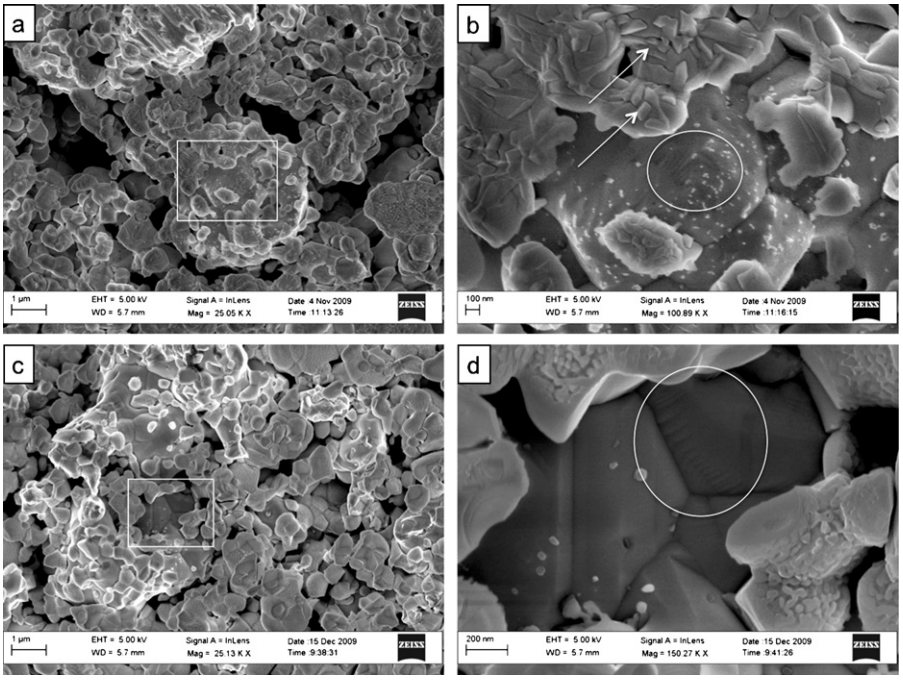

Fig. 3. SEM SE images of a Ni/CGO anode from cell operated in moist H_2/N_2 for 24 h at 700 °C. (a and b) Plan view images; (b) is a magnified view of the highlighted region in (a). (c and d) Cross-section images; (d) is a magnified view of part of the region in (c).

Cells were operated at 700 °C in moist H_2/N_2 for ~24 h and representative SEM microstructures are shown in Fig. 3. The CGO grains exhibit considerable surface relief in the plan view orientation (indicated by arrows in Fig. 3b). This is likely an artifact due to contact between the anode and the current collector, as the surface structure is not present throughout the thickness of the anode (Fig. 3d). All subsequent SEM images are cross-section orientations in order to avoid any confusion from this contacting effect. CGO particles, similar to those shown in Fig. 1 are present on many of the Ni grains. There is some evidence of Ni terracing for this condition, as shown in Fig. 3b and d (circled regions), but these regions were rare and difficult to find.

Fig. 4 shows cross-section images of cells (near the centre of the anode) operated for a total of about 25 h with exposure to H_2S. The sample in Fig. 4a was exposed to moist H_2/N_2 with 0.5 ppm H_2S for 15 h, while the sample in Fig. 4b was exposed to moist H_2/N_2 with 1.0 ppm H_2S for 18 h. Nickel terracing was not extensive for the sample exposed to 0.5 H_2S, but still more prevalent than for the control sample. If the H_2S concentration and exposure time were increased (1 ppm and 18 h), terracing was easier to find on Ni grains and the extent of terracing was much more pronounced (Fig. 4b). It appears then that Ni terracing is enhanced by exposure to H_2S.

To our knowledge, the work presented by Lohsoontorn [16] was the first to show terracing or faceting of Ni grains in Ni cermet anode structures. However, Ni terracing, or for that matter terracing of other metals, is not a new phenomenon; there are several instances reported in the literature in the 1970s and early 1980s. (e.g., [18,19]). Loier and Boos [18] studied Ni–S alloys containing 100 or 1000 ppm sulphur by weight annealed at elevated temperatures. Obviously, there are two major differences relative to this work, i.e., the sulphur concentrations were much higher and Ni–S alloys were produced – Ni was not exposed to a sulphur-containing atmosphere. After annealing the Ni–S alloys at 1200 °C, striations or terraces were observed on the Ni surfaces [18]. The terracing was much more pronounced and on a larger scale (striation spacings were on the order of 1 μm) than that observed here (~tens of nm), which is likely a result of the higher S concentration and higher annealing temperatures. Loier and Boos considered terracing to be a non-equilibrium phenomenon – annealing resulted in sulphur segregation to Ni grain boundaries, which are internal surfaces. Samples were reheated to 1200 °C to allow all the sulphur to go back into solid solution in the Ni (solubility increases with increasing temperature). When the samples were quenched to room temperature, no terracing occurred since the sulphur was trapped in solid

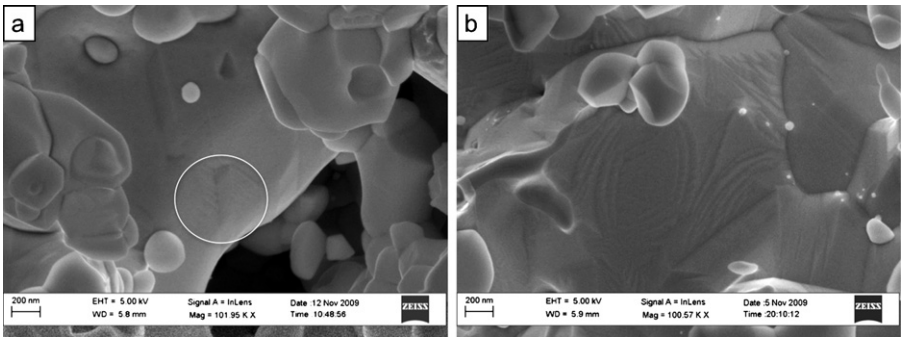

Fig. 4. SEM cross-section SE images of a Ni/CGO anode from cell operated under various conditions. (a) Moist H_2/N_2 with 0.5 ppm H_2S at 200 mA cm^{-2} and 700 °C; (b) moist H_2/N_2 with 1.0 ppm H_2S at 200 mA cm^{-2} and 700 °C. Faceted Ni grains are highlighted in (a).

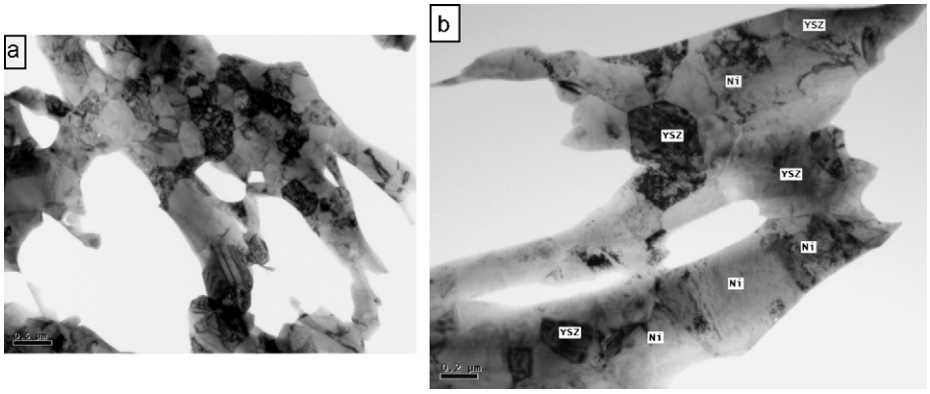

Fig. 5. TEM BF images of as reduced Ni/YSZ anode thin foil sample: (a) lower magnification image and (b) higher magnification image.

solution. However, if the alloy was slow cooled from 1200 °C to room temperature, terracing reappeared, since sulphur was able to come out of solution and re-segregate to Ni grain boundaries. Terracing is not unique to Ni or to sulphur impurities. The phenomenon was also observed for other elements (Bi and Te) alloyed with Ni [18].

In addition to Ni terracing, Rellick et al. [19] in an earlier paper showed terracing of grain boundaries in an Fe–Te (0.02 wt.%) alloy slowly cooled from elevated temperatures; this was also attributed to segregation (Te in this case) to grain boundaries. They also found sulphur segregation in the alloy (a common impurity in steels found in higher levels than in today's steels), which may have also contributed to terracing. The facets did not appear to form preferentially on a particular grain orientation. The driving force for impurity segregation is a reduction in the grain boundary energy, so that certain orientations may be energetically more favourable leading to terracing. Other elements, such as Sb, Sn, As and P, were found to have similar effects.

3.2. TEM analysis of YSZ/Ni anodes

Thin foil anode samples (YSZ/Ni) were exposed to H_2S-containing and H_2S-free atmospheres. These samples have a much higher surface to volume ratio than standard bulk anodes. The reason for studying these samples was to speed up the kinetics for Ni reconstruction, thereby providing some insight into long-term operation effects on the anode (in particular Ni) microstructure.

As a first step, as reduced YSZ/Ni TEM samples were examined before exposure. Typical lower and higher magnification images are shown in Fig. 5. The microstructure was typical of an anode cermet, with good contact between the YSZ and Ni grains and porosity due to the reduction of NiO to Ni, as well as from Ar sputtering. The Ni grains were close to cuboidal in shape with grain lengths and widths in the 300–500 nm range and thicknesses in the 100–150 nm range. YSZ grain sizes were similar in size, although slightly smaller. Assuming a Ni grain width/length of ~500 nm and a thickness of ~150 nm, the surface (including free surface, Ni grain boundaries and Ni/YSZ phase boundaries) to volume ratio is

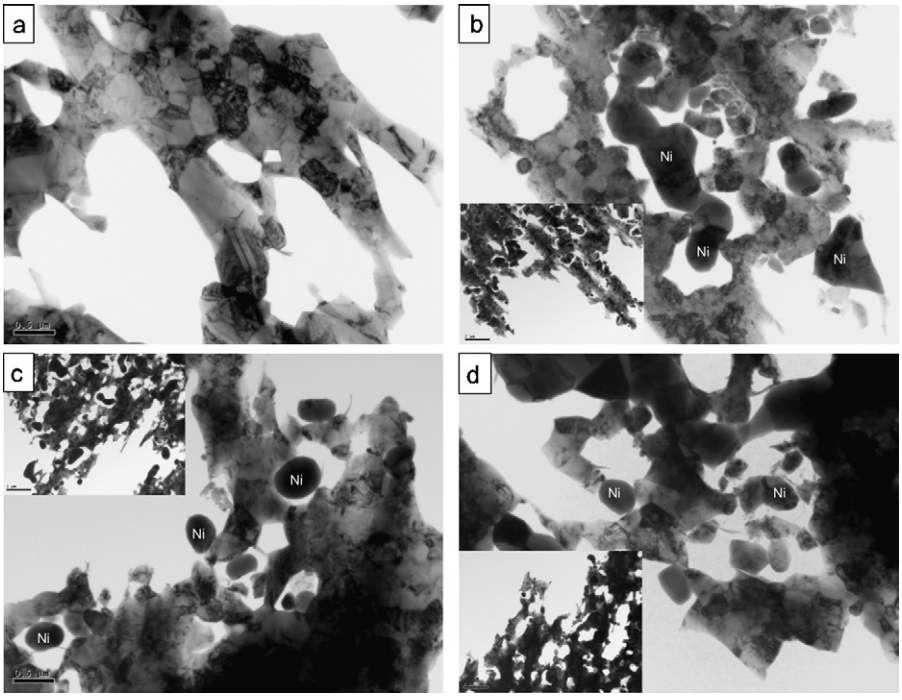

Fig. 6. TEM BF images of Ni/YSZ anode thin foil samples: (a) as reduced; (b) exposed at 700 °C to 50% H_2/50% N_2 with 1 ppm H_2S for 5 min; (c) exposed at 700 °C to 50% H_2/50% N_2 with 1 ppm H_2S for 15 min; exposed at 700 °C to 50% H_2/50% N_2 with 1 ppm H_2S for 90 min. Lower magnification images for each are shown in the insets.

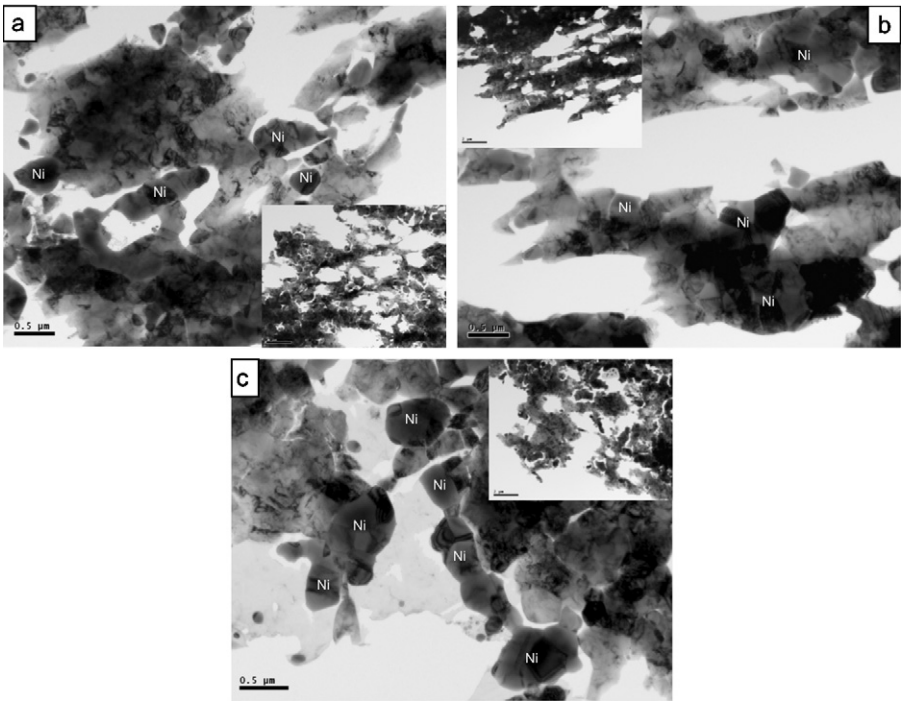

Fig. 7. TEM BF images of Ni/YSZ anode thin foil samples exposed to varying levels of H_2 for 15 min at 700 °C: (a) 2% H_2/98% N_2; (b) 10% H_2/90% N_2; (c) 100% H_2. Lower magnification images for each are shown in the insets.

$\sim$0.021 $nm^2\ nm^{-3}$ of which at least 60% is free surface, i.e., directly exposed to the atmosphere (assuming only the top and bottom surfaces are exposed to the atmosphere). By way of comparison, a bulk anode, with grains of the same diameter ($\sim$500 nm), and assuming a shape close to a tetrakaidecahedron, would have a surface to volume ratio of 2.37/d (d is the grain size) [20] or $\sim$0.0047 $nm^2\ nm^{-3}$. The thin foil anode then has about 4.5 times more Ni surface per unit volume than the bulk anode. The relative increase in the amount of free surface would likely be even larger for the thin foil sample compared with the bulk sample.

Restructuring of the Ni in the anode was observed for all annealing environments; however, the extent was dependent on the gaseous environment and annealing time. Low magnification TEM bright field (BF) images for annealing in dry H_2 with 1 ppm H_2S are shown in Fig. 6; the as reduced sample is shown for comparison in Fig. 6a. Significant changes have occurred to the Ni, even at annealing times as low as 5 min (Fig. 6b). Nickel grains have agglomerated; they are easy to differentiate from the YSZ grains as they tend to exhibit darker contrast since agglomeration has resulted in a local increase in thickness. At longer annealing times (15 and 90 min. – Fig. 6c and d), several Ni grains have completely detached from the YSZ/Ni framework and dropped out.

To determine whether the agglomeration process was related to the presence of H_2S in the annealing environment, or just a consequence of heating to a high temperature ($\sim$0.56 of the absolute melting temperature of Ni), YSZ/Ni anodes were annealed in other environments at the same temperature. Low magnification images for samples annealed in different concentrations of dry H_2 (balance is N_2) for 15 min are shown in Fig. 7. It is clear that Ni agglomeration has occurred for these samples; however, two main observations are evident. First of all, the amount of agglomeration is dependent on the H_2 concentration in the annealing environment. Agglomeration has just begun for samples annealed in 2% H_2, but has become more extensive in 100% H_2. Secondly, the amount of agglomeration for the same annealing time (15 min) is less pronounced for the sample annealed in pure H_2 (Fig. 7c) compared with the sample annealed in H_2 with a small amount of H_2S (1 ppm – Fig. 6c). Therefore, Ni agglomeration occurs in H_2 environments with and without H_2S, but the presence of H_2S enhances the kinetics of agglomeration.

Returning to the first observation (extent of Ni agglomeration depends on H_2 concentration), a recent paper reports agglomeration and faceting for Ni thin films (5–30 nm in thickness) deposited on SiO_2 and annealed in H_2/Ar for 1 h at 700–950 °C [20]. The Ni self-assembled into hexagonal shapes at temperatures greater than 800 °C, with more rounded structures and less faceting at <800 °C. The H_2 concentration in the gas affected the self-assembly process; agglomeration and faceting were more pronounced as the H_2 concentration was increased from 0% (pure Ar) to pure H_2. Faceted particles had large flat tops parallel to {1 1 1} planes (lowest surface energy – lower by $\sim$20% compared with {1 0 0} and {1 1 0} planes). The authors proposed that self-assembly of Ni films into particles with {1 1 1} flat tops is driven by thermodynamics (lower surface energy). In hydrogen, the increase in volume free energy due to hydrogen dissolution in Ni further drives the self-assembly process – i.e., the process is enhanced in H_2. In addition, the loss of adhesion between the Ni and underlying SiO_2 was attributed to the low thermal conductivity (1.3–1.4 $W\,m^{-1}\,K$) for SiO_2, leading to excessive heating at the interface. There may be a similar effect for the Ni/YSZ interface or the Ni/CGO interface; thermal conductivities for Ni, YSZ and CGO are 91 $W(m\,K)^{-1}$, 2 $W(m\,K)^{-1}$ and 2–3 $W(m\,K)^{-1}$, respectively. The latter point will be discussed further in subsequent paragraphs.

Coarsening of Ni in anodes has been reported to be enhanced by the presence of steam in the fuel gas, although the degree of agglomeration does not appear to depend on the water content [5,8]. As such, water was added to the gas environment to evaluate its effect on agglomeration. TEM BF images of samples annealed for 15 min in H_2 or H_2 with 1 ppm H_2S, with and without steam (2% H_2O), are shown in Fig. 8. The presence of steam appears to speed up the agglomeration process for both H_2S-containing and H_2S-free H_2. A larger portion of the Ni in the samples has agglomerated to such an extent that many Ni grains have dropped out of the cermet structure.

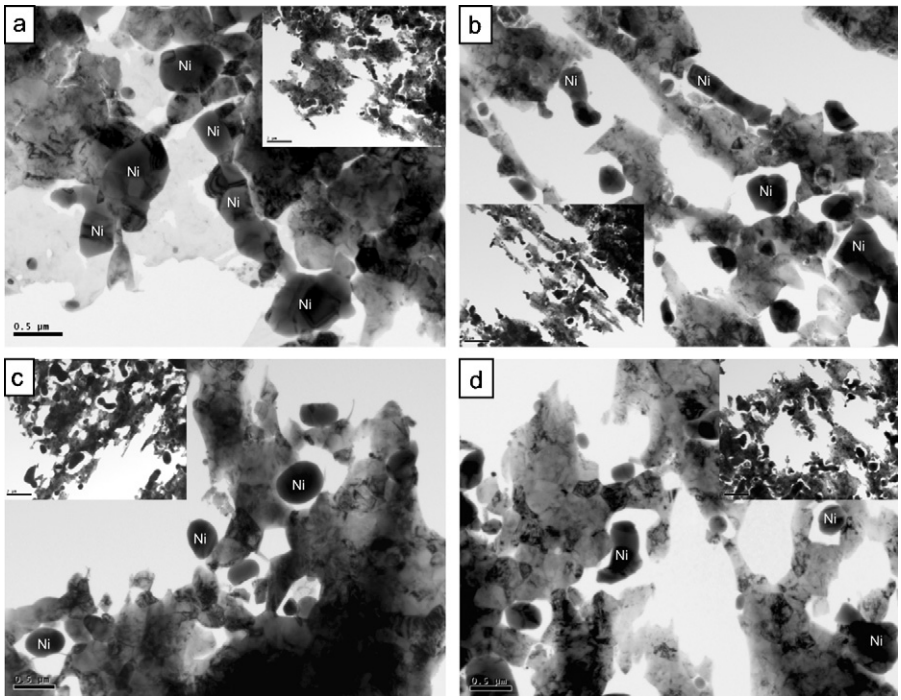

Fig. 8. TEM BF images of Ni/YSZ anode thin foil samples exposed to various atmospheres for 15 min at 700 °C: (a) 100% H_2; (b) 98% H_2/2% H_2O; (c) 100% H_2 + 1 ppm H_2S; (d) 98% H_2/2% H_2O + 1 ppm H_2S. Lower magnification images for each are shown in the insets.

To summarize the above results, it is apparent that Ni in the composite anode structure will agglomerate at fuel cell operation temperatures (e.g., 700 °C), which in itself is neither a new phenomenon nor a particularly surprising one, given that operating temperatures exceed 0.5 of the absolute melting temperature for Ni. As mentioned above and cited in numerous references, Ni coarsening and agglomeration in fuel cell anodes is a concern. The presence of the ceramic constituent (YSZ in this case) helps to alleviate this problem somewhat. The geometry of the TEM samples (high surface/volume ratio) increases the kinetics of restructuring, which may provide some insight into long-term operation effects of actual anodes. The relative effects of the anode atmosphere have been demonstrated: Ni agglomeration is enhanced by increased H_2 concentrations in the fuel and by the presence of both H_2S and H_2O. The above analysis, while not quantitative, does provide qualitative insights into agglomeration.

One goal of this paper is to determine any link between the Ni faceting observed in the anodes (Ni/CGO) from actual fuel cells operated under various conditions and the Ni restructuring observed in the TEM samples of Ni/YSZ anodes. Before continuing, it should be noted that agglomeration of Ni in cermet anodes is not restricted to Ni/YSZ cermets, but was also observed in TEM samples prepared from the Ni/CGO anode (not shown here). TEM samples of the Ni/YSZ anodes were examined in the SEM in order to search for any signs of the same kind of terracing observed for bulk Ni/CGO anodes. An example of one such sample is shown in Fig. 9a (pure H_2 + 1 ppm H_2S exposed for 15 min at 700 °C), along with a Ni/CGO anode sample that had been operated in fuel with 1 ppm H_2S (Fig. 9b). Both images were taken at almost the same magnification. Nickel terracing is clearly visible for the Ni/CGO sample (Fig. 9b). The SEM image of the TEM sample was taken several tens of microns away from the edge of the hole in the TEM sample, i.e., the region observed in Fig. 9a represents a transition from a thin film to a bulk material. Interestingly, terraces on the Ni grains are readily apparent and these are on a similar scale to the terraces in Fig. 9b. This is clear evidence that terracing does not require a current load. In addition, terracing may be a precursor to agglomeration. The TEM samples were studied more closely in an effort to provide support for this claim.

The samples exposed to varying levels of H_2 were examined first, since agglomeration was less pronounced, particularly at low H_2 levels. Fig. 10 shows images from a sample exposed to 10%

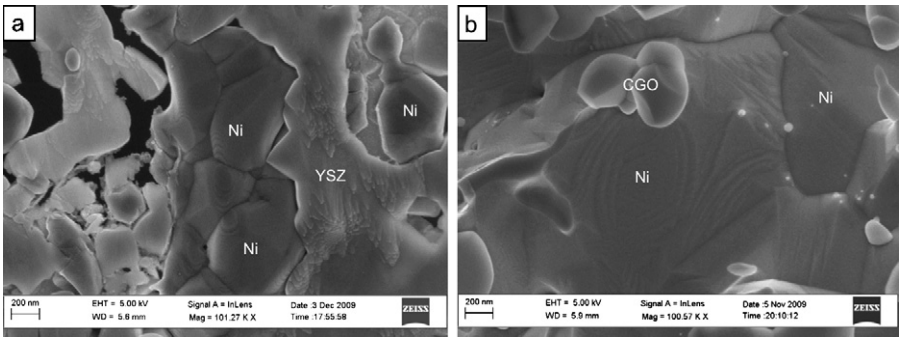

Fig. 9. SEM SE images showing faceting of Ni surfaces. (a) Ni/YSZ TEM sample exposed to H_2 with 1 ppm H_2S at 700 °C for 15 min; (b) Ni/CGO anode from a cell operated at 200 mA cm^{-2} in moist H_2 with 1 ppm H_2S.

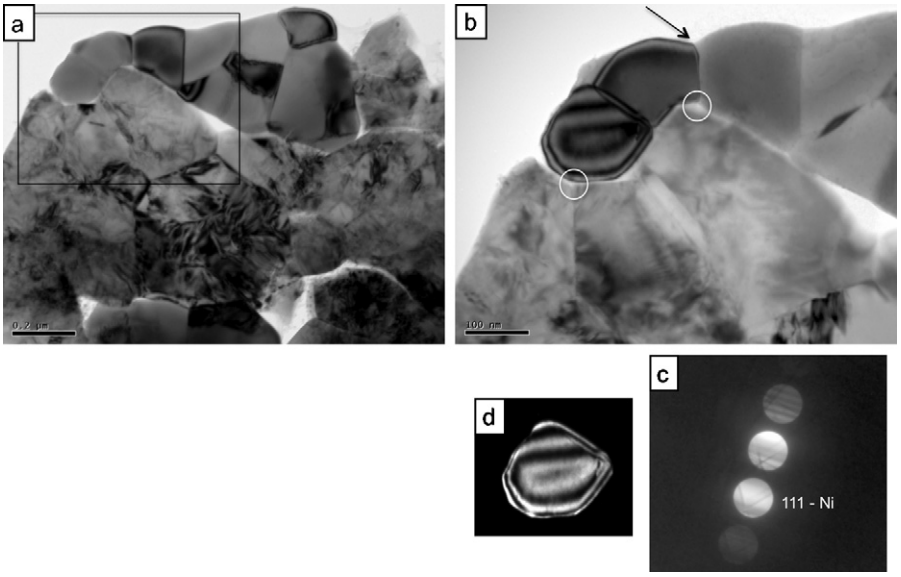

Fig. 10. Thin foil example exposed to 10% H_2/90% N_2 at 700 °C for 15 min. (a) Lower magnification BF image; (b) higher magnification BF image of sample in (a) tilted to a two-beam condition for one of the Ni grains; (c) microdiffraction pattern from Ni grain exhibiting thickness fringes; (d) DF image of Ni grain with thickness fringes.

H_2/90% N_2 for 15 min at 700 °C – equivalent to the condition in Fig. 7b. Fig. 10a shows a BF image of a region with several Ni grains in the top portion of the image; these are bordered on the bottom and right hand side by YSZ grains. The region indicated in Fig. 10a has been expanded and tilted so that one of the Ni grains is strongly diffracting (Fig. 10b), i.e., a two-beam condition (see the microdiffraction pattern from the grain in Fig. 10c). This is the grain that exhibits the periodic fringes, also known as thickness fringes. The Ni grains are debonding from the YSZ grains and this begins at triple points, i.e., where some combination of three Ni/YSZ grains meet (examples are circled in Fig. 10b). In addition, Ni has begun the agglomeration process, as evidenced by thermal grooving effects at Ni grain boundaries (indicated by the arrow in Fig. 10b). The distribution of thickness fringes, i.e., radiating out from the centre, for the strongly diffracting Ni grain in Fig. 10b indicates that the grain has faceted, which is more clear in the dark field (DF) image in Fig. 10d taken using the 1 1 1 reflection for Ni. The shape of the Ni grains will be addressed in subsequent paragraphs.

Another region from the same sample is shown in Fig. 11. A lower magnification image, showing the overall microstructure, is given in the inset. The main image is a magnified view of the region marked, showing a partially restructured Ni grain surrounded by YSZ grains. Debonding between the Ni grain and the YSZ grains is evident, and the debonding again begins at triple points. The sample has been tilted to a strongly diffracting condition for the Ni (two-beam condition) and a similar distribution of thickness fringes is present (as in Fig. 10), again denoting faceting of the Ni grain. Microdiffraction patterns are shown for the Ni and surrounding YSZ grains. There is no orientation relationship between Ni and any of the neighbouring Ni, which indicates that restructuring is not orientation dependent.

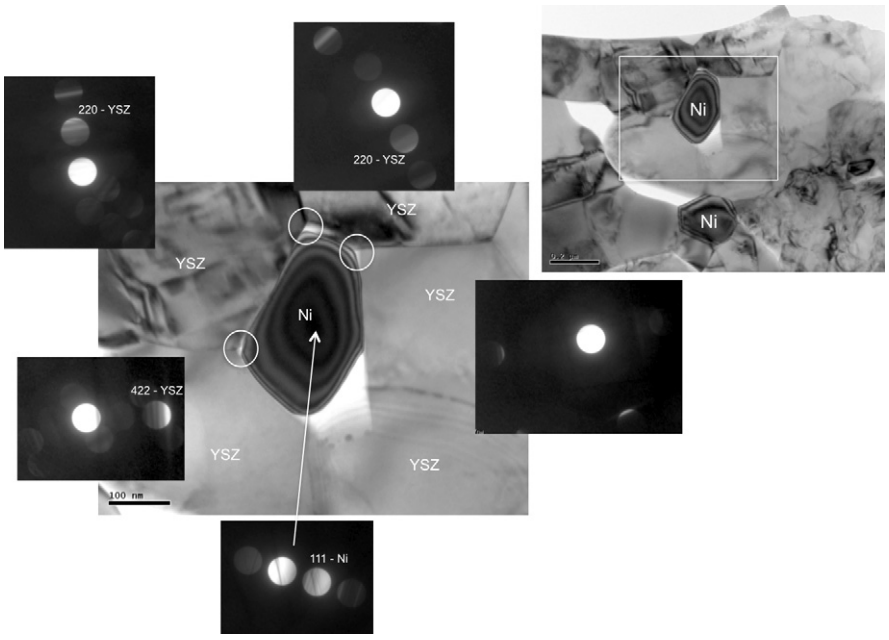

Fig. 11. TEM BF images and microdiffraction patterns from indicated grains of thin foil example exposed to 10% H_2/90% N_2 at 700 °C for 15 min.

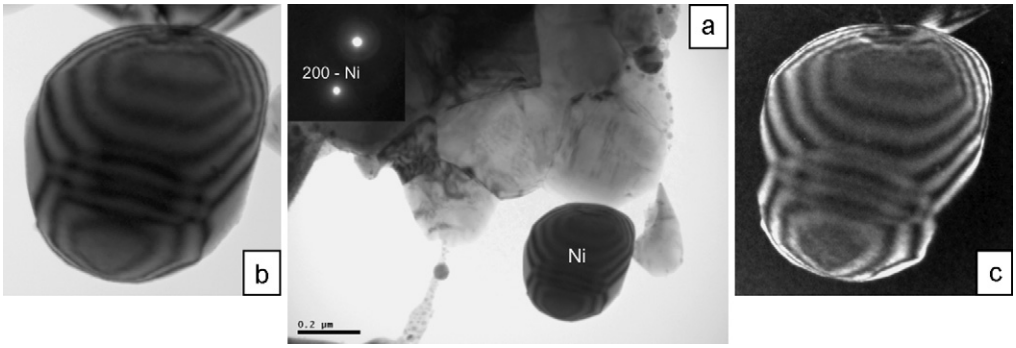

Fig. 12. Thin foil sample exposed to 100% H_2 plus 1 ppm H_2S at 700 °C for 15 min. (a) Lower magnification BF image showing Ni grain almost fully detached from YSZ grains, with Ni diffraction pattern in the inset; (b) higher magnification BF image of Ni grain in (a); (c) DF image of Ni grain.

Additional examples for other annealing environments are shown in Fig. 12 (H_2 plus 1 ppm H_2S) and Fig. 13 (98% H_2/2% H_2O plus 1 ppm H_2S). The Ni grain in Fig. 12 has almost completely detached from the surrounding YSZ. Two sets of concentric thickness fringes are visible in the BF (Fig. 12b) and DF (Fig. 12c) images. The sample in Fig. 13a shows two adjacent Ni grains almost fully detached from the YSZ and restructured. Tilting to different two-beam conditions reveals thickness fringes for each of the Ni grains. Fig. 13b shows a magnified view (both BF and DF) of the left hand Ni grain, while Fig. 13c shows a magnified view (both BF and DF) of the right hand Ni grain. Thickness fringes are also visible at the boundary between the two Ni particles, indicating a tilted grain boundary.

The thickness fringes mentioned above are a direct result of Ni grain restructuring. Thickness fringes are a diffraction contrast effect that arise due to variations in sample thickness across the region of interest. These fringes are easiest to interpret when the region of interest has been tilted to a two-beam (the unscattered and one strongly diffracting beam) condition as done here. If a sample is wedge shaped, periodic light/dark fringes will appear at regular intervals corresponding to specific thicknesses, which are multiples of the electron extinction distance for a given reflection [22]. Given the distribution of thickness fringes, i.e., they radiate out from the centre towards the Ni grain edges, the restructured Ni grains have a faceted, polyhedral shape. The driving force for the formation of these shapes is likely a reduction in the surface energy. All things being equal, a spherical shape would be expected; however, a polyhedral shape is favoured because of a preference for low energy surfaces such as the {1 1 1} type planes for fcc metals. The facet angles can be estimated from the electron extinction distances (~33 nm and ~38 nm for the 1 1 1 and 2 0 0 reflections, respectively [22]) and the fringe spacings; values ranging from 50° to 70° were

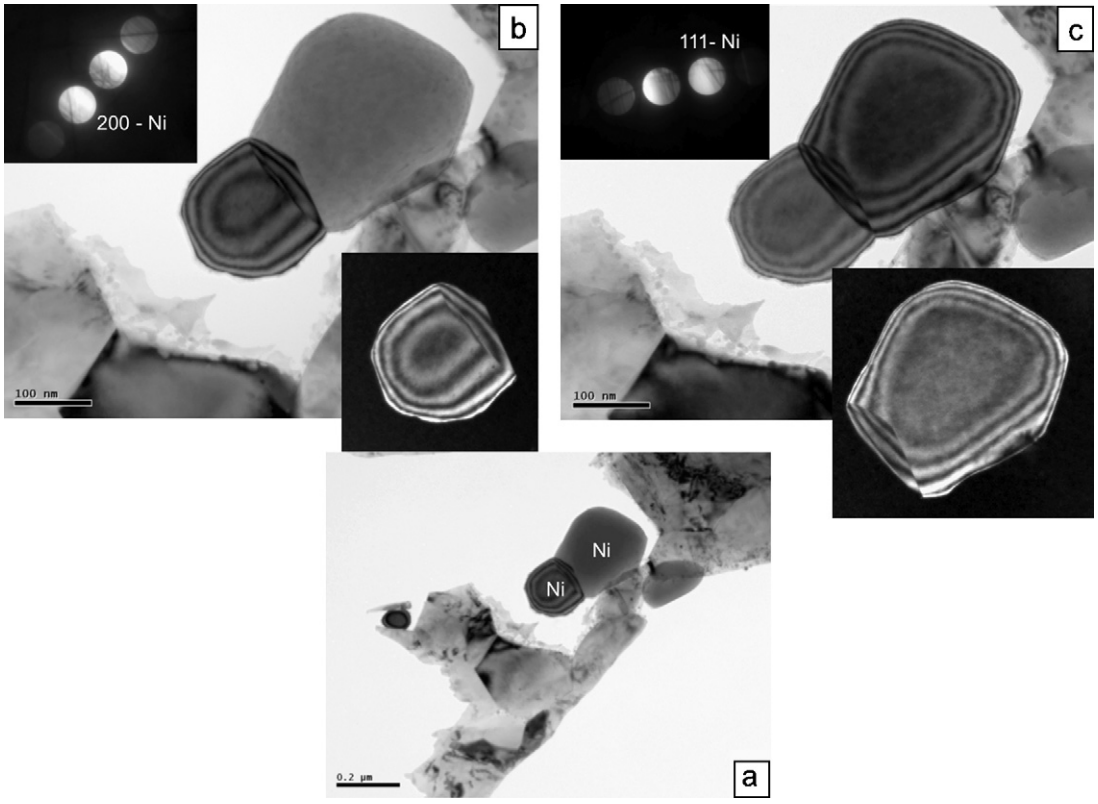

Fig. 13. Thin foil sample exposed to 98% H_2/2% H_2O plus 1 ppm H_2S at 700 °C for 15 min. (a) Lower magnification BF image showing two Ni grains detached from surrounding YSZ grains; (b) higher magnification BF image of Ni grains in (a) with left grain tilted to a two-beam condition – DF image of left grain is also shown; (c) higher magnification BF image of Ni grains in (a) with right grain tilted to a two-beam condition – DF image of right grain is also shown.

obtained. The angle between two different {1 1 1} planes is ~70°, while the angle between {1 1 1} and {1 0 0} planes is ~55°, both of which fall within the estimated range.

To confirm the proposed shapes in the preceding paragraph, an exposed TEM sample was re-examined in the SEM. Electron transparent regions of the sample shown in Fig. 9a (exposed to H_2 for 15 min at 700 °C) were imaged (using SEs) and a representative image is shown in Fig. 14a. This region is adjacent to the hole in the TEM sample and shows several Ni particles within a thin matrix of YSZ. Many of the Ni particles are <200 nm in size, so that they are electron transparent. The polyhedral shape is evident, particularly for the circled particles. A TEM BF image, at about the same magnification, from the same sample (similar morphology but different area) is shown in Fig. 14b. Restructured Ni particles within a thin YSZ matrix are present. Also visible in Fig. 14b is a "string" of Ni particles that has detached from the surrounding YSZ. In addition, two relatively large Ni grains (>500 nm in size) are visible at the top of the image in Fig. 14a. These grains are at an earlier stage of restructuring and clearly display the same type of terracing seen for Ni grains in bulk Ni/CGO anodes.

As final evidence for Ni restructuring, electron tomography was performed on Ni particles in the sample annealed for 15 min at 700 °C in 1 ppm H_2S (balance is H_2). One example is shown in Fig. 15. A series of images were taken from a given particle at 1–2° intervals over the angular range of −60° to +60°; the HAADF image at 0° tilt is shown in Fig. 15a. The particle has almost completely detached from the adjacent YSZ grain. Two views of the reconstructed, three-dimensional image are shown in Fig. 15b and c. The image in Fig. 15b is close to the same orientation as that in Fig. 15a, while the image in Fig. 15c has been rotated 35° in a counterclockwise direction about the axis depicted by the arrow. There is some distortion in the reconstructed images due to limited angular range (120°) of the imaging data; however, the faceted nature of the particle is clear.

Agglomeration can lead to loss of active surface area and reduced anode electronic conductivity. As mentioned previously, debonding accompanied by agglomeration of Ni thin films on SiO_2 was observed by Kim et al. [21], who attributed the effect to the large thermal conductivity difference between Ni and SiO_2. A similarly large difference exists between Ni and YSZ (as well as Ni and CGO). Restructuring also depends on the wetting characteristics of Ni on the ceramic phase. For Ni droplets on YSZ in a 4% H_2–Ar atmosphere, just above the melting temperature for Ni (~1500 °C), the contact angle is quite large (112–117°) [23,24] which is indicative of poor wettability. The Ni/YSZ interfacial energy is quite large

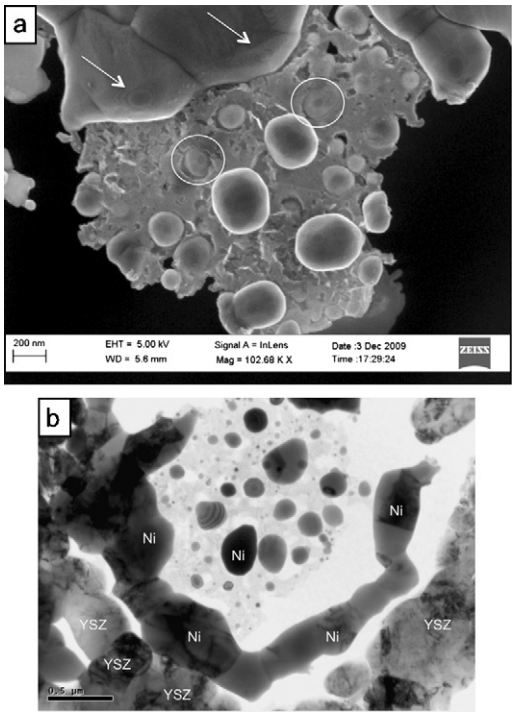

Fig. 14. (a) SEM SE image of thin foil sample exposed to 100% H_2 at 700 °C for 15 min. A region adjacent to the hole is shown. (b) TEM BF image of thin foil sample exposed to 100% H_2 at 700 °C for 15 min.

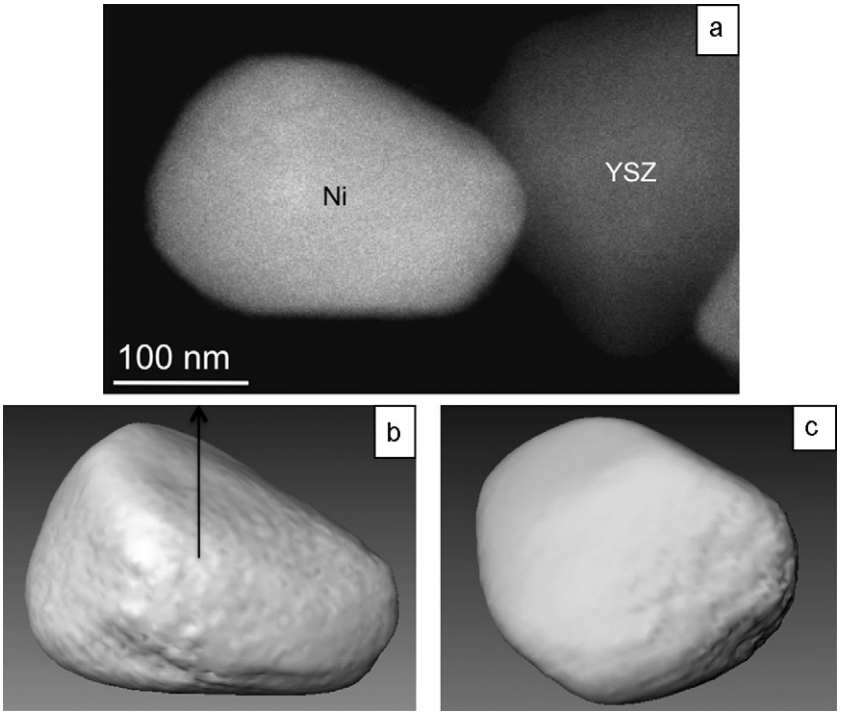

Fig. 15. (a) HAADF image showing restructured Ni particle attached to a YSZ grain. (b and c) Two-dimensional views of a reconstructed image of the particle in (a); the image in (c) is rotated 35° counterclockwise relative to the image in (b), about the direction depicted by the arrow.

at 0.96–1.1 J m^{-2} [23,24]. At lower temperatures (1250 °C) in the same environment, debonding of Ni from YSZ was reported and was attributed to the large difference in thermal expansion coefficients (TEC) [23,24]. Two separate surfaces (YSZ and Ni) appeared to be more favourable thermodynamically than a shared Ni/YSZ interface.

4. Conclusions

The effects of gaseous environment on the microstructure of solid oxide fuel cell anodes were studied using electron microscopy techniques. Two types of anodes were characterized, i.e., Ni/CGO anodes from bulk cells and thin foil Ni/YSZ anodes. Significant changes occurred to the Ni component of the cermets and these are summarized as follows:

1. Terracing of Ni grains in the anode (Ni/CGO) occurred for all cells operated at 700 °C and 200 mA cm^{-2} in H_2S-containing and H_2S-free moist H_2. Terracing prevalence increased with increasing H_2S levels.
2. Large scale restructuring of Ni grains was observed for thin foil anodes (Ni/YSZ). This was characterized by agglomeration and faceting of Ni grains and eventual detachment from YSZ. The extent of restructuring increased with increasing H_2 levels and the presence of moisture and/or H_2S in the gas.
3. Terracing was observed in both bulk and thin foil anodes, with or without current load, and appears to be a precursor to Ni agglomeration.

Acknowledgements

The authors wish to thank the UK EPSRC for funding this work under the programme “New Research Directions for Solid Oxide Fuel Cell Science and Engineering” EP/F009720/1. The assistance provided by Dr. James Perkins of Imperial College London with the tomographic imaging (FEI Titan 80/300 TEM/STEM) and image processing is also acknowledged. One of the authors (D. Ivey) would like to acknowledge the support of the University of Alberta for granting a sabbatical leave during which time this work was completed.

References

[1] L. Carrette, K.A. Friedrich, U. Stimming, Fuel Cells 1 (1) (2001) 5–39.
[2] H. Yokokawa, N. Sakai, T. Horita, K. Yamaji, Fuel Cells 1 (2) (2001) 117–131.
[3] K. Sasaki, K. Susuki, A. Iyoshi, M. Uchimura, N. Imamura, H. Kusaba, Y. Teraoka, H. Fuchino, K. Tsujimoto, Y. Uchida, N. Jingo, J. Electrochem. Soc. 153 (11) (2006) A2023–A2029.
[4] N.F.P. Ribeiro, M. Souza, O.R.M. Neto, S.M.R. Vasconcelos, M. Schmal, Appl. Catal. A: Gen. 353 (2) (2009) 305–309.
[5] W.Z. Zhu, S.C. Deevi, Mater. Sci. Eng. A 362 (2003) 228–239.
[6] S. Zha, W. Rauch, M. Liu, Solid State Ionics 166 (2004) 241–250.
[7] S.P. Jiang, J. Mater. Sci. 38 (18) (2003) 3775–3782.
[8] D. Simwonis, F. Tietz, D. Stover, Solid State Ionics 132 (3–4) (2000) 241–251.
[9] T. Iwata, J. Electrochem. Soc. 143 (5) (1996) 1521–1525.
[10] C. Bartholomew, Appl. Catal. A: Gen. 212 (2001) 17–60.
[11] G. Israelson, J. Mater. Eng. Perform. 13 (3) (2004) 282–286.
[12] Y. Matsuzaki, I. Yasuda, Solid State Ionics 132 (2000) 261–269.
[13] Y. Matsuzaki, I. Yasuda, in: H. Yokokawa, S.C. Singhal (Eds.), The Electrochemical Society Proceedings Series, Pennington, NJ, USA, 2001, pp. 769–779.
[14] D. Waldbillig, D.G. Ivey, A. Wood, 44th Annual Conference of Metallurgists COM, Calgary, AB, August 21–24, 2005, pp. 237–249, Published in Proceedings, Fuel Cell and Hydrogen Technologies, D. Ghosh (Ed.), MetSoc.
[15] P. Lohsoontorn, D.J.L. Brett, N.P. Brandon, J. Power Sources 183 (2008) 232–239.
[16] P. Lohsoontorn, The Impact of Sulphur on Ni-based Anodes for Solid Oxide Fuel Cells, PhD Thesis (Ph.D. and D.I.C.), Imperial College London, 2008, 232 pp.
[17] G. Offer, P. Shearing, J. Golbert, D.J.L. Brett, A. Atkinson, N.P. Brandon, Electrochim. Acta 53 (26) (2008) 7614–7621.
[18] C. Loier, J.Y. Boos, Met. Trans. A 12A (1981) 129–135.
[19] J.R. Rellick, C.J. McMahon Jr., H.L. Marcus, P.W. Palmberg, Met. Trans. 2 (1971) 1492–1494.
[20] R.T. DeHoff, F. Rhines, Quantitative Microscopy, McGraw-Hill, New York, 1968.
[21] K.J. Kim, Y.J. Yun, S. Ji, J.-H. Lee, D.H. Ha, J. Nanosci. Nanotechnol. 9 (2009) 4786–4791.
[22] D.B. Williams, C.B. Carter, Transmission Electron Microscopy: A Textbook for Materials Science, Plenum Press, 1996.
[23] A. Tsoga, A. Naoumidis, P. Nikolopoulos, Acta Mater. 44 (9) (1996) 3679–3692.
[24] J.G. Duh, W.S. Chien, B.S. Chious, J. Mater. Sci. Lett. 8 (1989) 405–408.